

# An anisotropic local modification of crystal field levels in Pr-based pyrochlores: a muon-induced effect modelled using density functional theory

F. R. Foronda,<sup>1</sup> F. Lang,<sup>1</sup> J. S. Möller,<sup>1,\*</sup> T. Lancaster,<sup>2</sup> A. T. Boothroyd,<sup>1</sup>  
F. L. Pratt,<sup>3</sup> S. R. Giblin,<sup>4</sup> D. Prabhakaran,<sup>1</sup> and S. J. Blundell<sup>1,†</sup>

<sup>1</sup>*Oxford University Department of Physics, Clarendon Laboratory, Parks Road, Oxford, OX1 3PU, United Kingdom*

<sup>2</sup>*Durham University, Centre for Materials Physics, South Road, Durham, DH1 3LE, United Kingdom*

<sup>3</sup>*ISIS Facility, Rutherford Appleton Laboratory, Chilton, Oxfordshire OX11 0QX, United Kingdom*

<sup>4</sup>*School of Physics and Astronomy, Cardiff University, Cardiff, CF24 3AA, United Kingdom*

(Dated: August 22, 2014)

Muon spin relaxation measurements on some quantum spin ice candidate materials, the insulating pyrochlores  $\text{Pr}_2\text{B}_2\text{O}_7$  ( $B = \text{Sn, Zr, Hf}$ ), have been performed for temperatures in the range 0.05–280 K. The results are indicative of a static distribution of magnetic moments which appears to grow on cooling and whose size at low temperatures is significantly larger than that expected for Pr nuclear moments. Using density functional theory we show how this effect can be explained via a hyperfine enhancement arising from a splitting of the non-Kramers doublet ground states on Pr ions close to the muon which itself causes a highly anisotropic distortion field. We provide a quantitative relationship between this effect and the measured temperature dependence of the muon relaxation and discuss the relevance of these observations to muon experiments in other frustrated magnetic materials.

PACS numbers: 76.75.+i, 75.10.-b, 75.40.Cx, 75.10.Jm

The muon-spin relaxation ( $\mu\text{SR}$ ) technique has been widely used as a probe of exotic magnetic behavior in frustrated systems [1]. A crucial question for these experiments is to what extent the presence of an implanted muon perturbs its local environment to such a degree that the measured response reflects the nature of the local distortions more than the physical behavior of the system under study. To answer this question we have identified a worst-case scenario, where the intrinsic magnetic behaviour is that of a quantum spin ice originating from the magnetic moments of  $\text{Pr}^{3+}$  ions. The ground state of this non-Kramers ion in a high symmetry site is particularly susceptible to modification by the implanted muon. By using density-functional theory (DFT) and crystal-field (CF) calculations, we show in this Letter how the observed behavior results from a highly anisotropic distortion field induced by the implanted muon.

In pyrochlore oxides  $\text{A}_2\text{B}_2\text{O}_7$ , in which the magnetic A ions occupy a lattice of corner-sharing tetrahedra, a variety of ground states can be realised, including spin glasses and spin ices [2]. Spin-ice behavior has been widely studied in  $\text{Dy}_2\text{Ti}_2\text{O}_7$  and  $\text{Ho}_2\text{Ti}_2\text{O}_7$  (i.e. with  $\text{A}=\text{Dy}$  or  $\text{Ho}$  and  $\text{B}=\text{Ti}$ ) and arises because the Ising spins are constrained by the CF to point in or out of each tetrahedron and along the local  $\langle 111 \rangle$  axes [3, 4]. It has been suggested that a new type of *quantum* spin ice [5] may be realised in which A is a lanthanide with fewer f electrons and a smaller magnetic moment, such as  $\text{Pr}^{3+}$  [6, 7]. This leads to a spatially extended 4f wave function with a greater overlap with the oxygen 2p orbitals, as well as a weaker magnetic dipolar interaction (proportional to the square of the moment size) between nearest-neighbour sites. This can allow quantum tunneling between different ice configurations, thereby con-

verting the material from a spin ice to a quantum spin liquid. Like its classical counterpart, the most notable feature of this new state is that it is predicted to host unconventional excitations. These are linearly dispersive magnetic excitations (magnetic photons) which offer the possibility of constructing a real lattice analogue of quantum electromagnetism [8, 9]. The compound  $\text{Pr}_2\text{Ir}_2\text{O}_7$  has been identified as a highly correlated metallic spin liquid [10, 11] and a previous  $\mu\text{SR}$  investigation found behavior that was interpreted as being induced by the muon [12, 13], although the extent of the role of screening by the conduction electrons was not clear. We now demonstrate that this effect can be also found in the insulating compounds  $\text{Pr}_2\text{B}_2\text{O}_7$  ( $B = \text{Sn, Zr, and Hf}$ ) which are also candidate quantum spin ice systems, and we propose a mechanism for the observed effect.

Zero-field  $\mu\text{SR}$  measurements were carried out on polycrystalline samples using the EMU spectrometer at the ISIS muon facility, RAL. Data were taken in the temperature range 0.05–280 K using a  $^3\text{He}$  cryostat and  $^3\text{He}$ – $^4\text{He}$  dilution refrigerator. The samples were synthesised by standard solid-state reactions and confirmed by x-ray diffraction to be single phase. Representative raw spectra from  $\mu\text{SR}$  measurements taken in zero applied field at 1.5 K and 40 K are shown in Fig. 1. At 1.5 K all compounds show a Kubo-Toyabe relaxation function (an initially Gaussian depolarization which recovers to a  $\frac{1}{3}$  constant long-time tail) which can be understood as resulting from a distribution of randomly oriented, static magnetic moments [14]. The static moments lead to a Gaussian distribution of magnetic fields at the muon site of rms width  $B_{\text{rms}} = \Delta/\gamma_\mu$  where  $\gamma_\mu = 2\pi \times 135.5\text{MHz T}^{-1}$  is the muon gyromagnetic ratio. However, the value of  $\Delta$  extracted at low temperature is too large to originate

simply from nuclear spins. We fit our data to a product of a Gaussian Kubo-Toyabe function  $G_{KT}(\Delta, t)$  and a weakly relaxing exponential  $e^{-\lambda t}$ , the latter component to take into account some slow dynamics of the magnetic moments, and this fit function can be used across the entire temperature range studied. All samples show a small, rapidly-relaxing fraction which we interpret as a muonium state (and is responsible for the negative curvature in the asymmetry data at very short times), but we focus on the majority fraction in the subsequent discussion.

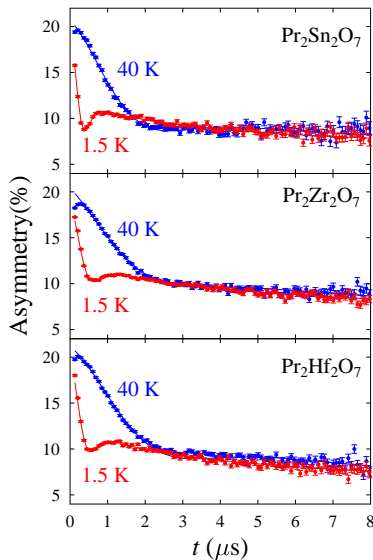


FIG. 1. Zero-field  $\mu$ SR spectra at 1.5 K and 40 K. Fits are to a Kubo-Toyabe relaxation function.

TABLE I. Lattice constants  $a$  (at 300 K),  $B_{\text{rms}}$  and fitted energy gaps for  $\text{Pr}_2\text{B}_2\text{O}_7$  ( $B = \text{Zr}, \text{Hf}, \text{Sn}$  and  $\text{Ir}$ ).  $\text{Pr}_2\text{Ir}_2\text{O}_7$  data taken from [10, 12].

compound	Zr	Hf	Sn	Ir
$a$ (Å)	10.7386(2)	10.7177(2)	10.6055(2)	10.3940(4)
$B_{\text{rms}}$ (mT)	3.76(6)	4(2)	5.65(5)	8.9(4)
$\epsilon_1$ (meV)	3.1(5)	2(2)	6(1)	0.5(1)
$\epsilon_2$ (meV)	0.6(1)	0.5(7)	0.6(1)	0.1(1)

The temperature dependences of the static width  $\Delta$  and dynamic relaxation rate  $\lambda$  are shown in Fig. 2. No magnetic transition can be seen throughout the measured temperature range; both parameters evolve smoothly, increasing steadily as the samples are cooled and the increase in  $\Delta$  can be interpreted as magnetic moments which grow with decreasing temperature. The two parameters  $\lambda$  and  $\Delta$  roughly track each other (see inset to Fig. 2), suggesting that the dynamics are related to these growing moments. The values of  $B_{\text{rms}}$  extrapolated to zero temperature (see Table I) are found to be an

order of magnitude larger than expected from  $^{141}\text{Pr}$  nuclear moments [12, 13] and are larger for smaller lattice constants  $a$ . Moreover, at low temperature we find that the relaxation decouples much more quickly in applied longitudinal fields than would be expected from the fitted values of  $B_{\text{rms}}$ .

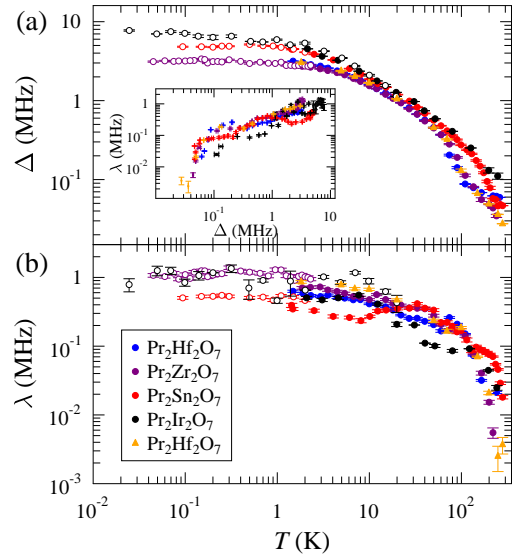


FIG. 2. Temperature dependences of (a)  $\Delta$  and (b)  $\lambda$  in Pr-based pyrochlores (helium cryostat, filled circles; dilution fridge, open circles). The two data sets for  $\text{Pr}_2\text{Hf}_2\text{O}_7$  were taken with the same sample but in separate experiments to check reproducibility. The  $\text{Pr}_2\text{Ir}_2\text{O}_7$  data are taken from [12].

In these quantum spin ice system we do not expect any static electronic moments at any temperature. Nuclear moments would be expected to give a small temperature-independent  $\Delta$ , but the observed behavior in Fig. 2(a) is both strongly temperature-dependent and at low temperatures very large. A likely explanation comes via a hyperfine enhancement of the Pr nuclear moments (as proposed for  $\text{Pr}_2\text{Ir}_2\text{O}_7$  [12, 13] and discussed in more detail below), but this mechanism requires a non-magnetic (singlet) ground state. In the pyrochlore structure the  $\text{Pr}^{3+}$  ( $4f^2$ ) ground state is a well-isolated non-Kramers doublet (confirmed in  $\text{Pr}_2\text{Sn}_2\text{O}_7$  and  $\text{Pr}_2\text{Zr}_2\text{O}_7$  by neutron spectroscopy [15, 16]) and this could be split by the distortion introduced by the muon. A muon-induced perturbation of the CF has been suggested previously in Pr-based intermetallics [17, 18], similarly associated with the splitting of the non-Kramers doublet. Since our data in insulating pyrochlores look very similar to that in metallic  $\text{Pr}_2\text{Ir}_2\text{O}_7$  we conclude that this mechanism is not susceptible to screening effects. In fact the carrier density in  $\text{Pr}_2\text{Ir}_2\text{O}_7$  is found to be rather low (estimated to be  $2.6 \times 10^{20} \text{ cm}^{-3}$ , i.e.  $\approx 0.02$  conduction electrons per Pr, from Hall effect measurements [10]). Moreover,  $\text{Pr}_2\text{Ir}_2\text{O}_7$  is believed to have a Fermi node at the  $\Gamma$  point [19], so that conduction electrons can only screen effec-

tively at very long wavelengths. Both considerations allow us to rationalise the insensitivity of this effect to the degree of metallicity.

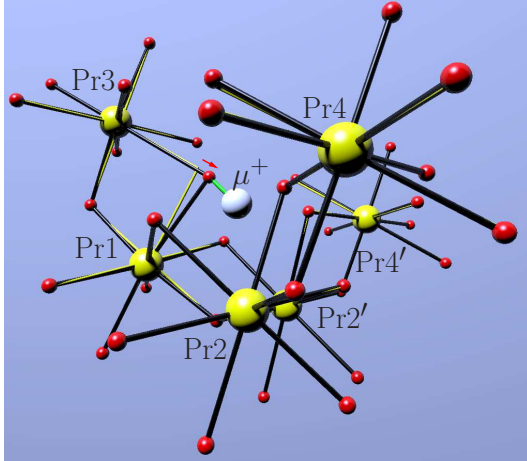


FIG. 3. Muon stopping site (white sphere) and atomic positions in  $\text{Pr}_2\text{Sn}_2\text{O}_7$  as calculated by DFT. Oxygen sites shown in red; Pr ions in yellow and bonds are shown as solid black lines. Bonds of the unperturbed lattice (yellow lines) are included for comparison. Pr ions are numbered in order of separation from  $\mu$  with Pr1 being the closest. The pair Pr2 and Pr2' are equidistant from the muon, as are Pr4 and Pr4'.

Although there has been previous evidence for a muon-induced effect in Pr-containing systems with a non-Kramers doublet [12, 17, 18], the nature of the effect has not been explored in detail. To address this issue we have used DFT calculations to determine the muon location and assess the effect of the muon on the local crystal structure and the CF of nearby Pr ions. The DFT calculations reported here were conducted with the plane-wave *Quantum Espresso* [20] program and utilized the generalized gradient approximation (GGA) exchange-correlation functional of Perdew, Burke and Ernzerhof [21] to locate potential muon sites. Ions were modeled using ultrasoft pseudopotentials and the muon was modeled by a norm-conserving hydrogen pseudopotential. This technique is known to give reliable results for muon sites in condensed matter systems [22–24]. The effect of including the 4f electrons in valence in the Pr pseudopotential (which is computationally challenging) on the determined muon sites and bulk lattice parameters was found to be negligible and hence a Pr pseudopotential with the 4f electrons in the core was employed for the calculations described below. The calculations were performed for  $\text{Pr}_2\text{Sn}_2\text{O}_7$  in a supercell consisting of a single conventional unit cell containing 88 atoms, and with the total energy converged to at least  $1 \times 10^{-6}$  Ry/atom (where Ry is the Rydberg constant). A convergence test yielded the suitable wavefunction and charge density cutoffs of 50 Ry and 300 Ry respectively on a  $2 \times 2 \times 2$  Monkhorst-Pack  $k$ -space grid, which were then used in

all subsequent calculations. The calculated atomic positions and lattice parameter of the unperturbed bulk were within 2% of the experimental values reported in [25], demonstrating an excellent agreement with x-ray and neutron powder experiments. To determine the stopping site, a muon was introduced on a grid of low-symmetry positions and the system was allowed to relax until all forces were below  $10^{-3}$  Ry/a.u. and the change in energy between iterations was less than  $10^{-4}$  Ry. The calculations presented here focus solely on the diamagnetic muon state, for which the unit cell has a total charge of +1. The final relaxed positions were found to be the same in spin-polarized and non-polarized calculations.

Three potential stopping sites were identified. However, as two of these required configurations that were  $\sim 0.45$  eV and 0.9 eV higher in energy than that of the lowest state we conclude that the latter is the most plausible stopping site in our real system. In this scenario the muon forms a O–H type bond of length  $\approx 1$  Å. It is bonded to an  $\text{O}^{2-}$  ion which also bonds to two Pr ions, labelled Pr1 and Pr3 in Fig. 3 (the Pr ions in Fig. 3 are numbered in order of separation from the muon, with Pr1 being the closest). The implanted muon results in an anisotropic distortion of the crystal lattice. The muon pulls an  $\text{O}^{2-}$  away from the ion Pr3, resulting in a greatly extended Pr3–O bond. The Pr1–O bond is only slightly changed in length, but is bent round, resulting in an anisotropic distribution of  $\text{O}^{2-}$  ions around Pr1. As shown below, the largest change in CF ground state is found for Pr3, but we note that the environment around the ions labelled Pr2, Pr2', Pr4 and Pr4' are more gently modified.

TABLE II. Parameters derived from DFT calculations of muon-induced lattice perturbations in  $\text{Pr}_2\text{Sn}_2\text{O}_7$ . Values are shown for the four nearest-neighbour Pr ions.

Pr atom	1	2,2'	3	4,4'
Pr– $\mu$ separation (Å)	2.7	3.2	4.1	4.7
Relative contribution	1.0	0.62	0.30	0.19
Distortion of $\text{PrO}_8$ unit (Å)	0.23	0.07	0.56	0.09
$\epsilon$ (meV)	4.8	1.3	11.4	4.0

We quantify the relative distortion of a  $\text{PrO}_8$  unit as the rms of the differences in Pr–O bond lengths between the perturbed and unperturbed lattice and these are listed in Table II for each of the nearest sites. We have calculated the CF levels for all nearby  $\text{PrO}_8$  environments, taking into account the spatial arrangement of the eight nearest-neighbour oxygen anions around each Pr (the electrostatic field due to the muon itself was also included initially, but it was found to make little difference, and so was neglected for the calculations described here). We used a point-charge model, with effective charges on the O1 and O2 sites chosen to reproduce the measured CF spectrum [15]. For each Pr site, the presence of the muon

splits the non-Kramers ground state doublet into two singlets (Fig. 4). As expected, the largest splitting ( $\epsilon$ ) of the singlets is found for Pr3 (the splittings are listed in Table II). These calculations show that the most perturbed Pr ion is not the nearest to the muon (there are three closer Pr ions that are significantly less perturbed), reflecting the highly anisotropic nature of the induced distortion field. Thus we conclude from these calculations that the muon is surrounded by a number of close Pr ions in which the CF splitting varies considerably.

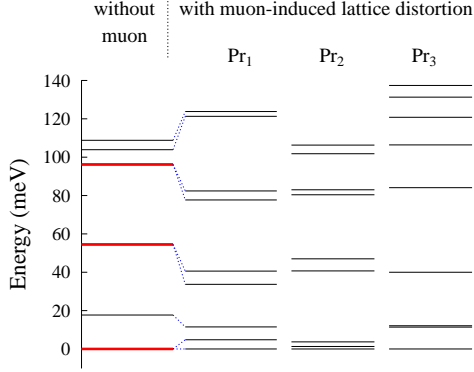


FIG. 4. Calculated CF levels of  $\text{Pr}^{3+}$  with and without muon-induced lattice distortion in  $\text{Pr}_2\text{Sn}_2\text{O}_7$ . Energies are calculated for three  $\text{Pr}^{3+}$  sites with varying degrees of distortion (see table II) as determined by DFT calculations. Bold red lines indicate doublets; plain black lines are singlets.

We now turn to the hyperfine enhancement of the Pr nuclear spins caused by these CFs. One can consider a two-state model due to Bleaney [26] in which the non-Kramers doublet is split into two singlets  $|G\rangle$  and  $|E\rangle$  by a small energy  $\epsilon$ . For a nucleus with spin  $I$  the hamiltonian takes the form

$$\mathcal{H} = \mathcal{H}_X + g_J \mu_B \mathbf{B} \cdot \mathbf{J} + A_J \mathbf{J} \cdot \mathbf{I} - g_I \mu_B \mathbf{B} \cdot \mathbf{I}. \quad (1)$$

Here the field  $\mathbf{B}$  is applied along the z-direction and  $\mathcal{H}_X$  accounts for the CF and the splitting  $\epsilon$ . There is an electronic matrix element  $\alpha = \langle E | \hat{J}_z | G \rangle$  where  $\hat{J}_z$  is the electronic angular momentum. This model allows an estimate of the magnetic moment  $m = k_B T (\partial \ln Z / \partial B)_T$  where  $Z$  is the partition function and yields

$$m = g_I \mu_B I_z + g_J \mu_B \alpha \sin \theta \tanh \left( \frac{\epsilon}{2 \cos \theta k_B T} \right) \quad (2)$$

where  $\tan \theta = 2\alpha(g_I \mu_B B_z + A_J I_z)/\epsilon$ . In zero-field  $\mu\text{SR}$  we take  $B_z = 0$  and hence

$$m = m_0 + \frac{\eta}{\tilde{\epsilon}} \tanh \left( \frac{\tilde{\epsilon}}{k_B T} \right) \quad (3)$$

where  $m_0 = g_I \mu_B I_z$ ,  $\eta = g_J \mu_B \alpha^2 A_J I_z$  and  $\tilde{\epsilon} =$

$\sqrt{(\epsilon/2)^2 + (\alpha A_J I_z)^2}$  (where  $\alpha^2 \leq J^2$ ). Taking  $\Delta \propto m$  with  $A_J/h = 1.093 \text{ GHz}$  [26] and  $I_z = \frac{5}{2}$  allows an estimate of the upper bound of  $\epsilon$ . The muon is coupled to many neighbouring moments by the dipole-dipole interaction which is proportional to  $r^{-3}$  (the relative contribution of this coupling for each site is listed in Table I, assuming a  $r^{-3}$  dependence). For simplicity, we choose a model in which there are dominant contributions to  $\Delta$  from two nearby moments which act in quadrature. We note that Eq. 3 implies that (neglecting the  $m_0$  component and for  $\epsilon \gg \alpha^2 A_J I_z$ ) the enhanced moment is approximately inversely proportional to  $\epsilon$  at low temperature, and therefore we expect the response to be dominated by nearby sites with small splittings. The zero-field data sets for both Sn and Zr compounds are found to fit well to this two-component model, see Fig. 5. We note that these values are within the same order of magnitude as our estimated splittings for the nearest neighbour sites Pr1 and Pr2/Pr2' for  $\text{Pr}_2\text{Sn}_2\text{O}_7$ . Given the sensitivity of the calculations to the precise distortion field, the restriction to two components, together with the limitations of the point-charge model of the CF, we believe this agreement is well within the inherent uncertainties.

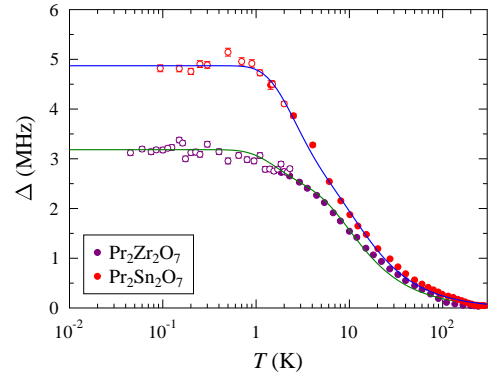


FIG. 5. Static relaxation rate  $\Delta$  in  $\text{Pr}_2\text{Sn}_2\text{O}_7$  and  $\text{Pr}_2\text{Zr}_2\text{O}_7$  fitted with the model described in the text.

To summarize, we have performed  $\mu\text{SR}$  measurements on Pr-based pyrochlores  $\text{Pr}_2\text{B}_2\text{O}_7$  ( $B = \text{Sn}, \text{Zr}, \text{Hf}$ ) in which any quantum spin-ice type behavior is masked by the presence of static, hyperfine-enhanced nuclear moments with weak dynamics which dominate the muon relaxation. This effect is due to a distribution of splittings of the non-Kramers doublet ground states of nearby Pr ions resulting from a highly anisotropic distortion field induced by the implanted muon. These observations show that, in certain circumstances,  $\mu\text{SR}$  experiments can measure a response which is dominated by the local distortion resulting from the implanted probe. This particular case is, however, very unusual since it relies on a splitting of a non-Kramers doublet and would be inoperable in systems in which a ground state degeneracy was



protected from such perturbations, such as  $\text{Dy}_2\text{Ti}_2\text{O}_7$ . Nevertheless, we expect that in muon experiments on other pyrochlore oxides a very similar anisotropic distortion field will inevitably be present, even if its effect is much more benign.

This work is supported by EPSRC (UK). The computations were performed on the Iridis cluster operated by the E-Infrastructure South Initiative. We thank Davide Ceresoli for helpful discussions and the provision of a Pseudopotential with 4f electrons in valence for cross-checking our results, and S. P. Cottrell at ISIS for technical assistance with the experiments.

---

\* Current address: Laboratory for Solid State Physics, ETH Zürich, Zürich, Switzerland

† [s.blundell@physics.ox.ac.uk](mailto:s.blundell@physics.ox.ac.uk)

- [1] P. Carretta and A. Keren, in *Highly Frustrated Magnetism*, edited by C. Lacroix, P. Mendels, and F. Mila (Springer, 2011) pp. 79–106.
- [2] J. S. Gardner, M. J. P. Gingras, and J. E. Greedan, *Rev. Mod. Phys.* **82**, 53 (2010).
- [3] S. T. Bramwell and M. J. P. Gingras, *Science* **294**, 1495 (2001).
- [4] C. Castelnovo, R. Moessner, and S. L. Sondhi, *Nature* **451**, 42 (2008).
- [5] M. J. P. Gingras and P. A. McClarty, *Reports on Progress in Physics* **77**, 056501 (2014).
- [6] S. Onoda and Y. Tanaka, *Phys. Rev. Lett.* **105**, 047201 (2010).
- [7] H. D. Zhou, C. R. Wiebe, J. A. Janik, L. Balicas, Y. J. Yo, Y. Qiu, J. R. D. Copley, and J. S. Gardner, *Phys. Rev. Lett.* **101**, 227204 (2008).
- [8] O. Benton, O. Sikora, and N. Shannon, *Phys. Rev. B* **86**, 075154 (2012).
- [9] S. B. Lee, S. Onoda, and L. Balents, *Phys. Rev. B* **86**, 104412 (2012).
- [10] S. Nakatsuji, Y. Machida, Y. Maeno, T. Tayama, T. Sakakibara, J. vanDuijn, L. Balicas, J. N. Millican, R. T. Macaluso, and J. Y. Chan, *Phys. Rev. Lett.* **96**, 087204 (2006).
- [11] Y. Tokiwa, J. Ishikawa, S. Nakatsuji, and P. Gegenwart, *Nature Materials* **13**, 356 (2014).
- [12] D. MacLaughlin, Y. Ohta, Y. Machida, S. Nakatsuji, G. Luke, K. Ishida, R. Heffner, L. Shu, and O. Bernal, *Physica B: Condensed Matter* **404**, 667 (2009).
- [13] D. E. MacLaughlin, Y. Nambu, Y. Ohta, Y. Machida, S. Nakatsuji, and O. O. Bernal, *Journal of Physics: Conference Series* **225**, 012031 (2010).
- [14] R. S. Hayano, Y. J. Uemura, J. Imazato, N. Nishida, T. Yamazaki, and R. Kubo, *Phys. Rev. B* **20**, 850 (1979).
- [15] A. J. Princep, D. Prabhakaran, A. T. Boothroyd, and D. T. Adroja, *Phys. Rev. B* **88**, 104421 (2013).
- [16] K. Kimura, S. Nakatsuji, J.-J. Wen, C. Broholm, M. B. Stone, E. Nishibori, and H. Sawa, *Nat Commun* **4** (2013).
- [17] R. Feyerherm, A. Amato, A. Grayevsky, F. Gygax, N. Kaplan, and A. Schenck, *Zeitschrift für Physik B Condensed Matter* **99**, 3 (1995).
- [18] T. Tashma, A. Amato, A. Grayevsky, F. N. Gygax, M. Pinkpank, A. Schenck, and N. Kaplan, *Phys. Rev. B* **56**, 9397 (1997).
- [19] L. Savary, E.-G. Moon, and L. Balents, ArXiv e-prints (2014), [arXiv:1403.5255 \[cond-mat.str-el\]](https://arxiv.org/abs/1403.5255).
- [20] P. Giannozzi, S. Baroni, N. Bonini, M. Calandra, R. Car, C. Cavazzoni, D. Ceresoli, G. L. Chiarotti, M. Cococcioni, I. Dabo, A. D. Corso, S. de Gironcoli, S. Fabris, G. Fratesi, R. Gebauer, U. Gerstmann, C. Gougoussis, A. Kokalj, M. Lazzeri, L. Martin-Samos, N. Marzari, F. Mauri, R. Mazzarello, S. Paolini, A. Pasquarello, L. Paulatto, C. Sbraccia, S. Scandolo, G. Sclauzero, A. P. Seitsonen, A. Smogunov, P. Umari, and R. M. Wentzcovitch, *Journal of Physics: Condensed Matter* **21**, 395502 (2009).
- [21] J. P. Perdew, K. Burke, and M. Ernzerhof, *Phys. Rev. Lett.* **77**, 3865 (1996).
- [22] J. S. Möller, D. Ceresoli, T. Lancaster, N. Marzari, and S. J. Blundell, *Phys. Rev. B* **87**, 121108 (2013).
- [23] F. Bernardini, P. Bonfà, S. Massidda, and R. De Renzi, *Phys. Rev. B* **87**, 115148 (2013).
- [24] S. J. Blundell, J. S. Möller, T. Lancaster, P. J. Baker, F. L. Pratt, G. Seber, and P. M. Lahti, *Phys. Rev. B* **88**, 064423 (2013).
- [25] B. J. Kennedy, B. A. Hunter, and C. J. Howard, *Journal of Solid State Chemistry* **130**, 58 (1997).
- [26] B. Bleaney, *Physica* **69**, 317 (1973).